Chapter 2
Nanoscale Materials: Fundamentals and Emergent Properties

Simona E. Hunyadi Murph, Kaitlin J. Coopersmith and George K. Larsen

Abstract As material size decreases into the nano size regime, novel properties arise that are different from their molecular and bulk counterparts. Due to the size and shape effects in this regime, a nanoparticle's morphology has a profound effect on its properties. This chapter addresses the effect of dimensionality on the optical, electronic, chemical, and physical assets of various nanomaterials and how physical and chemical relationships can be exploited to improve their properties. Delving into the nuances of the different sizes, shapes, and compositions gives one an appreciation of the potential that nanomaterials have to improve upon today's technologies. As scientists learn to fabricate increasingly more complex nanomaterials, new opportunities develop every day. A detailed discussion on the effect of morphology and nanometric dimensions on materials' physico-chemical properties, which lead to novel applications, will be covered in Chapter 5.

Keywords Anisotropy · Dimensionality · Shape-selective nanomaterials · Polarization · Crystalline anisotropy · Optical properties · Electronic properties · Chemical · Physical properties

2.1 Introduction

The design and controlled fabrication of colloidal materials with functional properties has flourished over the last few decades. The beauty and distinctiveness of nanoscale materials is rooted in their unique properties that emerge at the 1–100 nm scale. In this transitional regime, a material's physical, chemical, and biological properties may differ in fundamental ways from the properties of both bulk matter and the constituent atoms or molecules.

S.E. Hunyadi Murph (✉) · K.J. Coopersmith · G.K. Larsen
National Security Directorate, Savannah River National Laboratory, Aiken, SC, USA
e-mail: Simona.Murph@srnl.doe.gov

S.E. Hunyadi Murph
Department of Physics and Astronomy, University of Georgia, Athens, GA, USA

S.E. Hunyadi Murph et al. (eds.), *Anisotropic and Shape-Selective Nanomaterials*, Nanostructure Science and Technology, DOI 10.1007/978-3-319-59662-4_2

For decades, a staggering amount of research has focused on the creation of new nanomaterials and the elucidation of their unique property-structure correlations. Theoretical understanding of the mechanistic principles that govern the novel properties of the nanomaterials have also been studied extensively. Highly reliable bottom-up and top-down synthetic routes that produce increasingly complex nanomaterials with highly ordered and complex geometries have been developed. Complications in scaling up and uniformity that have hampered widespread application of nanomaterials in the early developments have been addressed to some extent. High throughput fabrication procedures amenable to scaling up for industrial scale implementation have been reported for many classes of nanoparticles.

A large variety of nanomaterials of various sizes (1–100 nm), shapes (including spheres, rods, cubes, triangles, wires, ribbons, nanotubes, and polygons), and compositions (fullerenes, to metal and semiconductor nanoparticles, to various designer molecules or a combination of both) with an array of different functionalities have been reported. Thorough discussions of these synthesis procedures are covered in detail in the next chapters. In this chapter, readers will be introduced to the fundamentals of inorganic nanostructures with an emphasis on noble metals, namely gold, silver and platinum materials. A more detailed discussion on fundamentals of other types of nanomaterials (metal oxides, other metals, hybrids and quantum dots) and how their properties affect their applications will be covered in Chap. 5.

In recent years, incorporation of nanomaterials in macro-devices opened the door to potential applications in nearly every sector of science and industry, particularly in medicine, biological sciences, electronic sensors, computing and microelectronics, environmental controls and remediation, transportation, energy production, chemical manufacturing, agriculture, and consumer products. According to the USA Environmental Protection Agency, nanomaterials can be found today in more than 1300 commercial products including medical equipment, textiles, fuel additives, cosmetics, plastics and more [1]. Nanomaterials are currently produced in metric tons per year and are expected to exponentially increase as new advances emerge [2, 3]. Scientists are relentlessly pursuing different routes to create nanomaterials and understand the physical and chemical relationship between composition, size, and morphology to incorporate nanomaterials into everyday life.

2.1.1 Dimensionality and Optical Properties

The unique properties of inorganic nanoparticles are often the result of their sizes being smaller than the mean free path of their electrons (10–100 nm) or the average distance an electron travels before being scattered (scattering length) [4–6]. At this scale, electrons are confined in one, two, or three dimensions, and quantum mechanical effects dominate the characteristics of matter [7, 8]. As a result, the physical and chemical properties of materials vary with nanoparticle size and shape, as demonstrated in Table 2.1 [4–9].

Table 2.1 Size and shape effects on gold nanoparticle's optical properties

Gold nanoparticles color	Shape	Size (nm)	λ (plasmon bands) (nm)
Brown	Sphere	1.5	520
Ruby-red	Sphere	20	525
Purple	Rod	D = 20 L = 40	520 580
Blue	Rod	D = 20 L = 57	520 620
Green	Rod	D = 20 L = 75	520 720
Brown	Rod	D = 20 L = 100	520 900

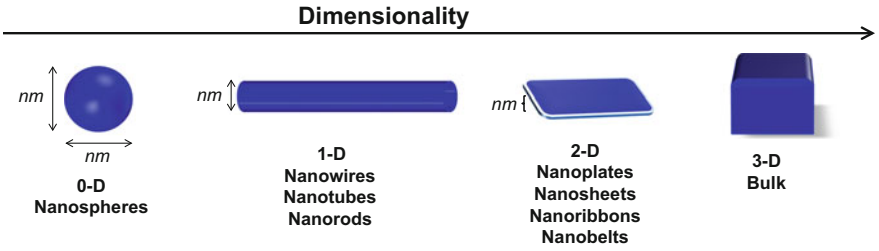

Fig. 2.1 Nanoparticle shape and dimensionality

Fundamentally, *isotropic* nanomaterials have properties and functionalities that do not depend on spatial orientation, while *anisotropic* nanomaterials have properties and functionalities that are determined by their orientation within the *x*, *y*, and *z* dimensions. These properties are directionally dependent on material geometry and orientation. Depending on these quantum confinement properties, nanoparticles are characterized as zero, one, two or three dimensional as demonstrated in Fig. 2.1.

All of the dimensions in zero dimensional nanostructures, or spheres, are in the nanometer size regime, so there is no electron delocalization. One dimensional structures have one dimension outside of the nanometer size regime that creates electron delocalization in one direction; the elongated axis allows for an increase in polarization and charge separation [7, 10]. This class of structure includes nanorods, nanowires, nanotubes, nanoribbons, and nanobelts [11]. Two dimensional nanoparticles are sheets or nano sized films that have two dimensions outside of the nanometer size regime. In these structures, electrons are confined in the thickness direction but not in the plane of the sheet. Three dimensional materials, or bulk materials, are not confined to the nanoscale in any direction; however, they may contain nanocrystalline structures or features that lead to interesting properties. This distinctive spatial behavior of anisotropic structures creates unexpected properties and applications that are not available in isotropic nanostructures. Ultimately, material properties can be tailored to a specific design and functionality by

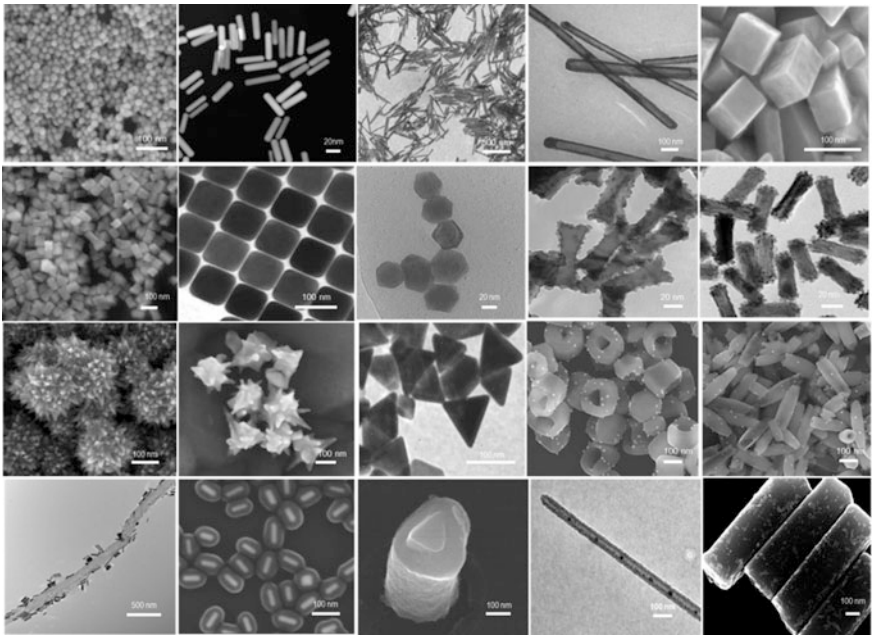

Fig. 2.2 SEM images showing a sample of the wide variety of nanoparticle shapes and sizes that can be made in our laboratory

controlling the geometry and structure of the nanometer scale structures [4–9, 12, 13]. Figure 2.2 shows a variety of different anisotropic structures that have been created in our laboratory.

Nanoparticles have high surface to volume ratios that lead to an increased fraction of atoms on the surface and fewer neighboring atoms [12]. This promotes distinctive structural and electronic changes. For example, a cube with a length of 1 m has a surface area of 6 m^2, while if this same cube was divided into a collection of smaller length cubes, each with lengths of 0.25 m, the surface area would increase to 24 m^2. Moreover, the atoms in the interior of a nanoparticle are more highly coordinated, and are therefore more stable than those at the nanoparticle surface [13, 14]. Subsequently, atoms on tips or corners of a crystal have more uncoordinated bonds and are more reactive than the edge or in-plane surface atoms. By simply decreasing the particle size, one could increase the number of surface atoms available for surface chemical reactions [12, 13]. The larger fractions of atoms at the particle surface of nanometer-sized materials promote faster reaction kinetics for various catalytic reactions. While gold is inert in its bulk form, as a nanoparticle of $\sim$3 nm, it catalyzes CO to CO_2 [6, 7, 15, 16]. Hollow nanoparticles serve as superior catalysts to their solid counterparts with the advantages of low density, increased surface area, and cost effective materials [12, 17].

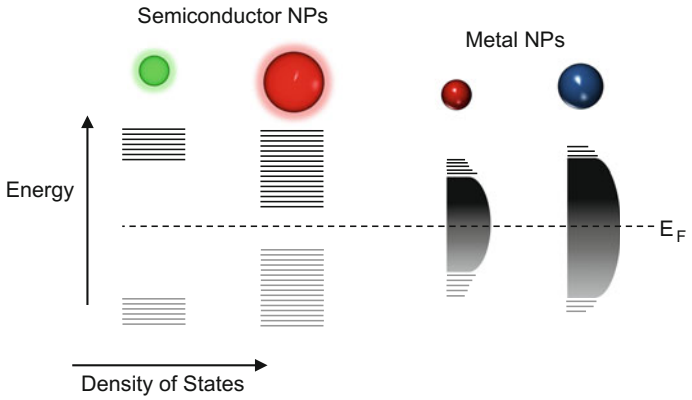

Fig. 2.3 Density of states and the location of the Fermi level (E_F) for semiconductor and metal nanocrystals

Since properties at the nanoscale are dictated by quantum mechanics, different architectures give rise to altered optical and electronic properties, which are affected by the degree of charge carrier quantum confinement, surface charge distribution and electron polarization along the various axes of the particles [18–21]. Due to the high surface to volume ratio, small surface changes, such as the binding or altering of binding events, can also lead to a significant change in the electrical and optical properties. This can lead to single molecule sensing [22].

Semiconductor nanocrystals, or quantum dots, can absorb and fluoresce in the ultraviolet to near-infrared regions of the electromagnetic spectrum. The optical properties of quantum dots are tailored by tuning the band gap, which is dependent on composition and size, as shown in Fig. 2.3. As the size increases, more atomic orbitals contribute to their density of states, leading to a smaller bandgap and a red-shift in absorption and emission. Asymmetry plays a large role in quantum dot optical properties, where photogenerated carriers can separate along longer axes, leading to a longer lifetime in the excited state [23, 24].

Unlike quantum dots, metallic nanoparticles have a continuous energy band that is responsible for their light absorption properties. Among many properties displayed by gold nanoparticles, one of the most notable is their ability to absorb and scatter light in the visible region of the electromagnetic spectrum [4–9, 12, 13, 25] as displayed in Fig. 2.4.

In metal nanoparticles, the number of the surface plasmon resonance (SPR) peaks generally increase as the symmetry of the particle decreases due to the increased polarization of the free electrons and surface charge distribution [18–20, 26]. For example, gold nanorods (AuNR) have two localized surface plasmon resonance (LSPR) bands due to the different absorption of the length and the width; [4–9, 12, 13, 25] the locations of these bands are tuned by changing the length and width of the rod [26]. Silver nanocubes can display multiple plasmon bands due to the accumulation of charges in the corners of the cube [20]. The plasmon band is

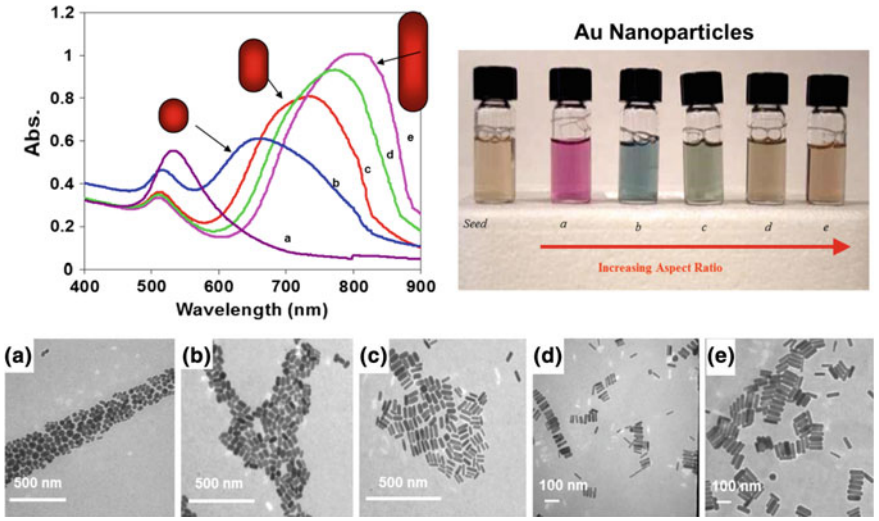

Fig. 2.4 Shape dependence of the optical properties of gold nanostructures. Transmission electron micrographs (*top*), optical spectra (*left*), and photographs of (*right*) aqueous solutions of gold nanorods of various aspect ratios. Seed sample: aspect ratio 1; sample **a**, aspect ratio ~1.4; sample **b**, aspect ratio ~2; sample **c**, aspect ratio ~3; sample **d**, aspect ratio ~3.50; sample **e**, aspect ratio ~4.4. *Scale bars* 500 nm for (**a**, **b**, **c**), and 100 nm for (**d**, **e**). Reprinted with permission from Ref. [6]. Copyright 2017 American Chemical Society

highly dependent on size, shape and refractive index, which have applications for LSPR sensing [4–9, 12, 13, 25, 27–30].

Nanoparticle shape dictates how sensitive the shift in the plasmon band is [25, 28] to changes in refractive index at the surface (Fig. 2.5), which can be exploited to detect the presence of most inorganic, organic and biological molecules and surface synthesis, catalysis and molecular binding events [6, 7, 9, 28, 31, 32]. These asymmetric properties can lead to the creation of more sensitive sensors, [32, 33] faster electronics, [34] more efficient energy storage devices [35] and better catalysts [12–14, 17, 36]. For intracellular delivery and imaging applications, [9, 27, 30] the kinetics of cellular uptake and the effect of nanoparticles on cellular functions is dependent on nanoparticle shape [37, 38].

2.1.2 Polarization and Anisotropy

Since most of the nanoparticles properties are highly surface dependent, morphology, composition and dimensionality have a profound effect on how nanoparticles interact with light [7, 25]. The sharp features of anisotropic shapes

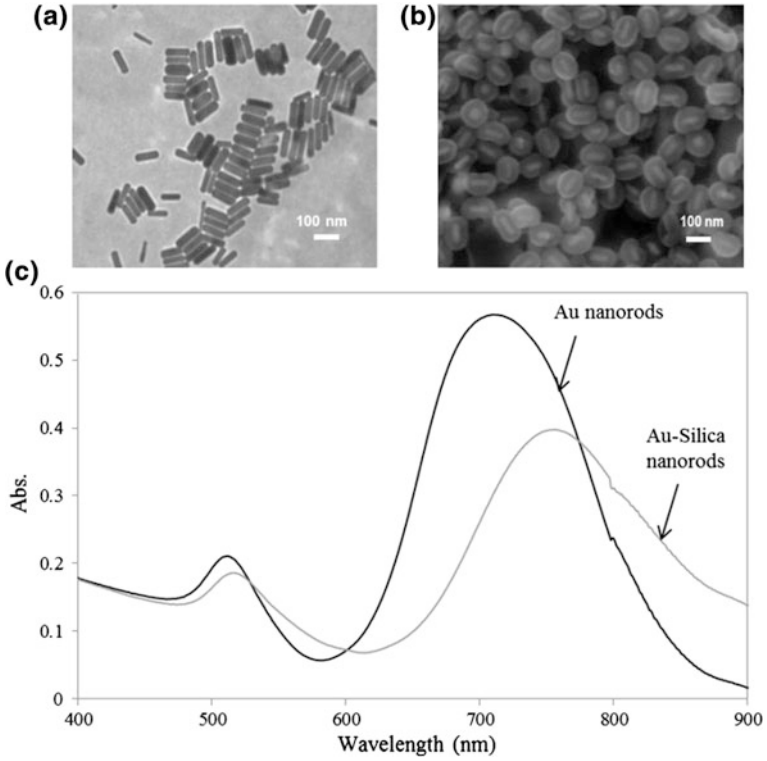

Fig. 2.5 **a** TEM image of Au nanorods, **b** SEM image of Au-silica core-shell nanorods, and **c** UV-Vis spectra of gold nanorods before and after coating with a silica shell

lead to locally enhanced electric fields that can act as "hot spots" for enhanced detection, light emitting diodes, and imaging [7, 28, 29]. Optical and magnetic properties are also controlled by the nanoparticle's anisotropy. Particles with an elongated axis, such as nanorods, have an increased charge separation that leads to an increase in catalysis and sensing efficiencies [39]. Anisotropic particles can polarize light. The degree and localization of the different planes of light is determined by the dimensions and morphologies, where the different light angles interact with the particles differently [21, 40–44]. In metal nanorods, the polarized light interacts with the longitudinal surface plasmon band, [44] whereas in spiky gold nanoshells, P-polarized light localizes on the tips of the cones and S-polarized light localizes on the regions at the bottom of the cones where the cones overlap [40]. Figure 2.6 shows finite difference time domain (FDTD) calculations for various gold nanorod shapes, where the maximum local electric field is related to the curvature [32]. The electric "hot spots" on the particles affect surface ligand bonding and optical responses [4–7, 28, 45].

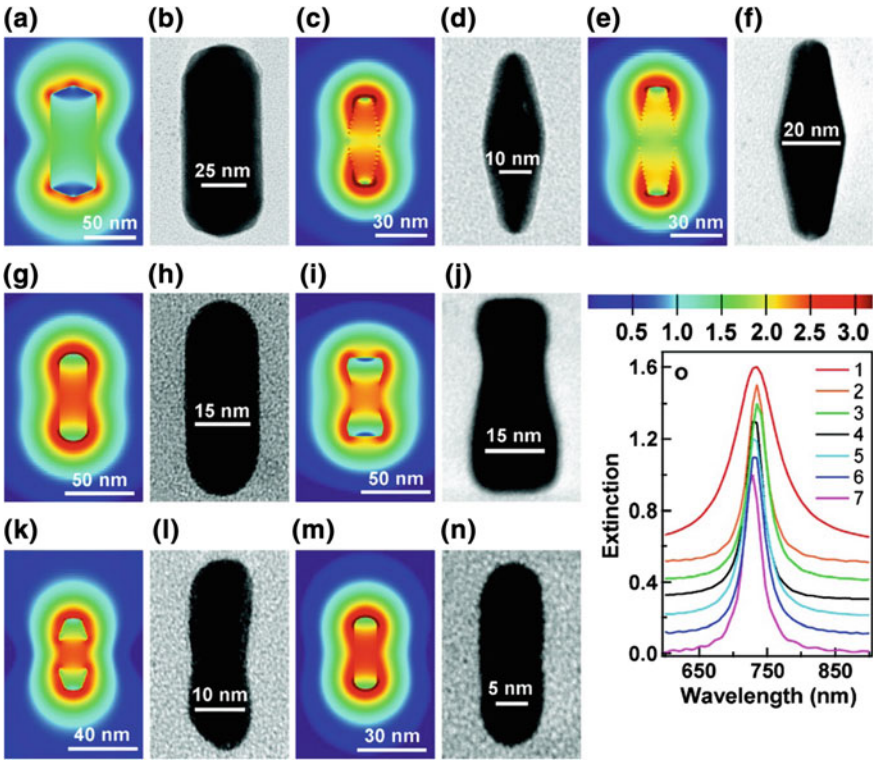

Fig. 2.6 Electric field intensity enhancement contours (*colored*) and TEM images (*gray*) of differently shaped Au nanocrystals: (**a**, **b**) Large NRs; (**c**, **d**) NBPs; (**e**, **f**) oxidized NBPs; (**g**, **h**) oxidized NRs; (**i**, **j**) dog-bone-like NRs; (**k**, **l**) peanut-like NRs; and (**m**, **n**) small NRs. (o) Calculated extinction spectra of Au nanocrystals embedded in water. *Curves 1* to *7* represent the large NRs, NBPs, oxidized NBPs, oxidized NRs, dog-bone-like NRs, peanut-like NRs, and small NRs, respectively. The field intensity enhancement is at the logarithmic scale. Reproduced with permission from Ref. [32]. Copyright © 2009 American Chemical Society

Polarization has an effect on electronic interactions; for example, the fluorophore emission of dyes attached to gold nanorods (or plasmon coupled gold nanoparticles) can become altered to match the absorption energy of the longitudinal plasmon for the anisotropic gold nanoparticle-dye conjugates, as shown in Fig. 2.7. This is attributed to the transition of the fluorophore from an excited state to a vibrational ground state close to the plasmon energy due to the enhancement from the local electric field from the plasmon resonance [42]. Polarization effects are dependent on polarization angle, so polarization studies can give information on the orientation of the nanoparticle, which is important for SERS, catalysis, biological imaging, among others.

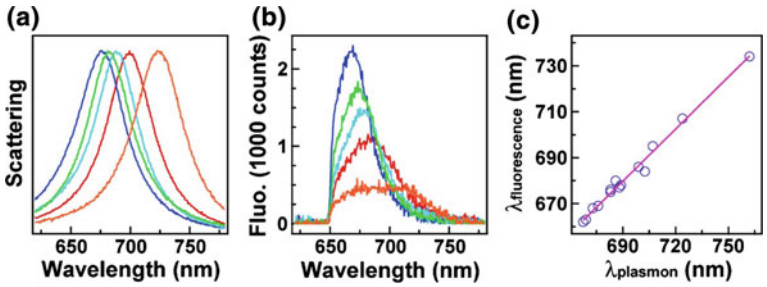

Fig. 2.7 Spectral shaping of the emission of oxazine 725. **a** Scattering spectra of the individual hybrid nanostructures containing the Au nanorods with different aspect ratios. **b** Corresponding fluorescence emission spectra. The emission spectra were recorded under the longitudinal polarization excitation. **c** Dependence of the fluorescence peak wavelength (empty circles) of oxazine 725 on the scattering peak wavelength. The line is a linear fit. Reproduced with permission from Ref. [42]. Copyright © 2009, American Chemical Society

2.1.3 Crystalline Anisotropy

Nanoparticle physico-chemical properties are also dependent on the interfacial atomic arrangement and coordination of the crystal. Generally, the density and symmetry of atoms in different crystallographic planes are not identical, and neither is their electronic structure, bonding, surface energy, or chemical reactivities [4, 5, 12].

The face-centered cubic crystalline lattice of single-crystal metal nanoparticles, namely gold, silver and platinum nanoparticles, typically have low-index facets: {100}, {111}, and {110} [8]. However, depending on the preparation conditions, namely surfactants, reduction agents, temperature, thermodynamic, and/or kinetic factors, etc., nanoparticles with different crystallographic facets, and subsequently, properties can be produced [4–7, 9, 12, 13, 25, 28, 30]. For example, gold nanorods of various dimensions, ~20 nm in diameter and up to 500 nm long, prepared in similar conditions through a seed mediated surfactant approach, have different crystallographic structures depending on the *presence* or *absence* of additive ions, e.g. Ag^+ (Fig. 2.8a–f). The diffraction pattern and the high resolution TEM images show that the short Au nanorods (~20 nm in diameter and up to 100 nm in length) prepared in the presence of the additive ions are single crystalline with no observable stacking faults, twins or volume dislocations [4, 5, 7]. High resolution TEM images of the short Au nanorods (Fig. 2.8d–f) show well-defined, continuous, and equally spaced fringe patterns for their atomic lattice. Surprisingly, a closer inspection of the long Au nanorods (~20 nm in diameter and up to 500 nm in length) prepared in the absence of the additive ions reveal a penta-twinned crystallographic structure with five well-defined facets typical of icosahedra structures (Fig. 2.8a–c) [20, 46].

The surfactant-directed approach is not the only procedure leading to penta-twinned crystals. Electron microscopy studies shows that silver nanowires up

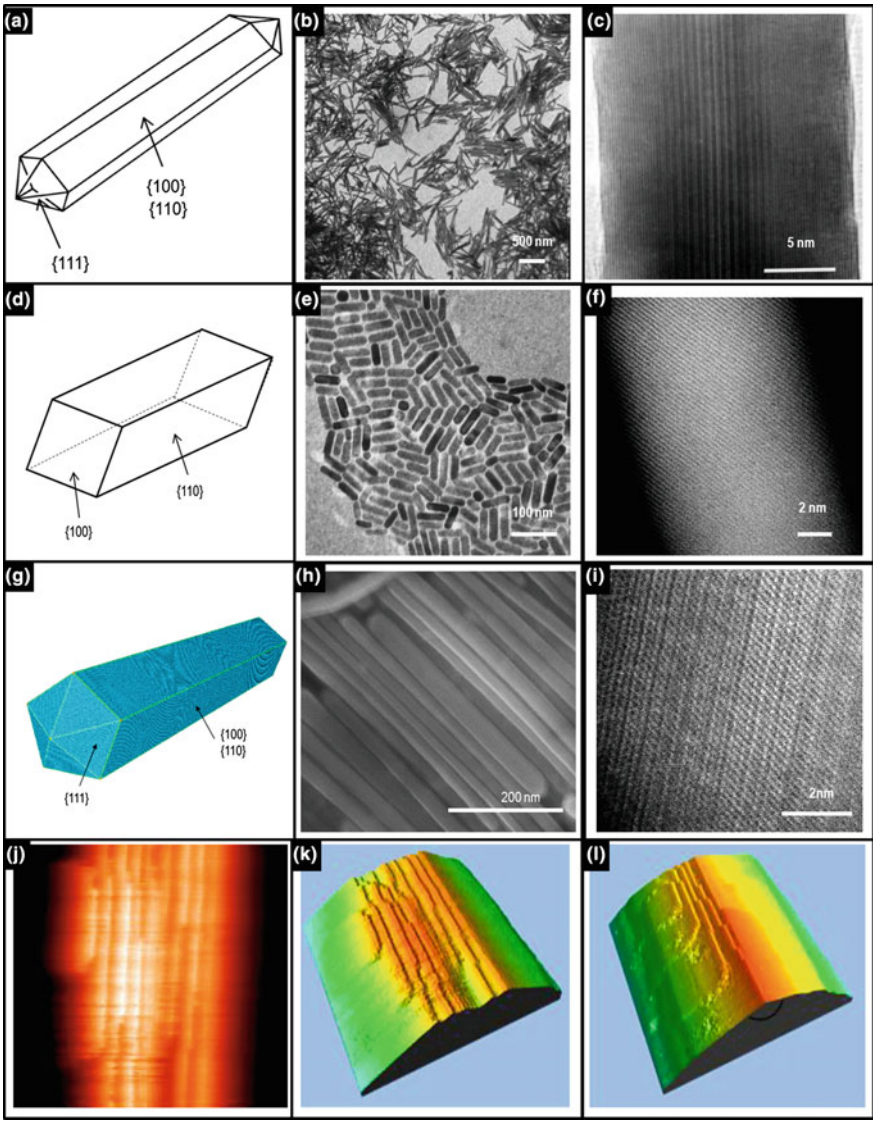
(a)
{100}
{110}
{111}
(b)
500 nm
(c)
5 nm
(d)
{110}
{100}
(e)
100 nm
(f)
2 nm
(g)
{100}
{110}
{111}
(h)
200 nm
(i)
2nm
(j)
(k)
(l)

◂**Fig. 2.8** (**a**–**c**) Gold nanorods prepared via a surfactant mediated approach in the absence of additive ions. **a** Cartoon of the penta twinned crystallography of Au nanorods, **b** TEM image of Au nanorods, **c** HRTEM of Au nanorods; (**d**–**f**) Gold nanorods prepared via a surfactant mediated approach in the presence of additive ions (Ag^+). (**a**) Cartoon of the single crystal Au nanorods, (**b**) TEM image of Au nanorods, **c** HRTEM of Au nanorods; (**g**–**l**) Ag nanowires prepared by an coarsening process via an oriented attachment mechanism. (**g**) Equilibrium atomic positions for a pentagonal nanowire with internal twins; (**h**) SEM image of Ag nanowires, (**i**) HRTEM image of penta-twinned Ag nanowire, (**j**) STM topography image, scale 20 · 20 nm2, of the top of the Ag nanowire, (**k**) 3 D rendering of Ag nanowires, (**l**) mage of another top section of the same wire, with the angle between the facets indicated with a black semicircle. (a) Reprinted with permission from Ref. [6]. Copyright 2017 American Chemical Society. (c) Reprinted with permission from Ref. [11]. Copyright 2017 American Chemical Society. (g) Reprinted with permission from Ref. [46]. Copyright 2017 American Chemical Society. (j-l) Reprinted with permission from Ref. [47]. Copyright 2017 with permission from Elsevier

to 10 nm long and 30 nm diameter prepared via a seedless method, in the absence of surfactants, also have penta-twinned crystallographic structures (Fig. 2.8g–l). Interestingly enough, these silver nanowires form through a coarsening process via an oriented attachment mechanism, which is completely different from the seed-mediated surfactant growth approach used to produce gold nanorods [7, 47, 48].

Ultimately, the crystallography of the final product is determined by the original "seed" nanoparticle, which can be tailored through the synthetic parameters [20, 49–51]. The crystallography of the "seed" [4–7, 9, 13, 46] (Fig. 2.9) can also determine the final nanoparticle shape, such as quantum rods versus tetrapods [49, 52] and silver spheres versus cubes or rods [20].

Crystallographic facet energies play a huge role in nanoparticle synthesis, applications, and properties [4]. In typical nanoparticle fabrication techniques, the final nanocrystal is truncated with the lowest energy facets, though this can be tuned through synthetic parameters and chemical etching [39, 53, 54]. Crystalline stability

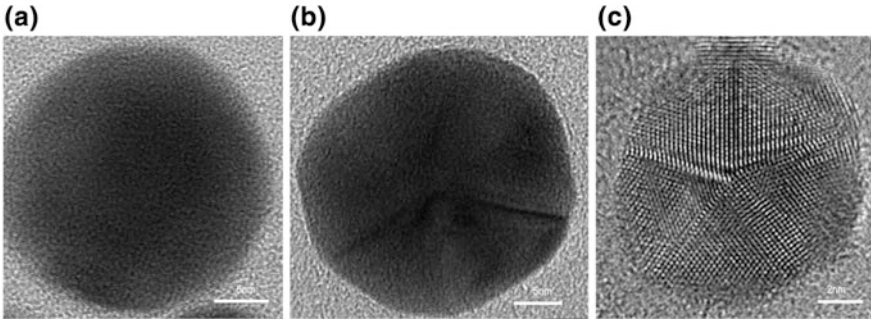

Fig. 2.9 HRTEM images of (**a**) single crystalline- Au nanospheres-"seeds", (**b**) penta-twined crystalline Au nanospheres, (**c**) penta twinned Ag nucleation centers. (**a**, **b**) Reprinted with permission from Ref. [13]. Copyright 2017 Springer. (**c**) Reprinted with permission from Ref. [46]. Copyright 2017 American Chemical Society

depends on the presence of dangling bonds, steps and terraces but this can also be tuned with facet specific capping agents. The manipulation of crystallographic stability is one aspect that drives the synthesis of anisotropic nanomaterials [50]. Multicomponent nanoparticles, such as core/shell and Janus nanoparticles, typically require a common crystallographic orientation (i.e. small lattice mismatch) to increase the binding stability between the two materials. Facet-selective etching is also used to dissolve the least stable facets, leading to the creation of nanoparticles with interesting morphologies such as hollow nanocubes [54]. Binding energy differences on certain facets is an important factor for chemical reactions and has been exploited to improve their efficiency and selectivity for applications such as catalysis, [55, 56] SERS, [57] and sensing [4, 7, 28, 45, 58]. The relative stability of crystallographic planes for surface based applications becomes increasingly important for anisotropic nanoparticles, which may contain elongated crystallographic planes and multiple different types of exposed facets.

It is important to consider how nanoparticle shape and crystalline properties relate to one another and how they impact the emergent properties of a nanoparticle. As described above, building nanoparticles from the bottom up typically depends on the manipulation of the energetics of the crystalline surfaces, and as a result, the final nanoparticle shape depends on the orientation of these crystalline planes with respect to each other. This is one reason that metallic nanocubes are fairly common the {100}, {110}, and {111} crystalline facets that form the faces, edges and corners, respectively, are typically very stable. However, for catalysis, high index facets are more reactive and desirable, and therefore different shapes are synthesized by promoting the growth of higher index facets. For example, highly catalytic Au nanoparticles enclosed by {830} and {730} facets correspondingly take the form of concave and convex nanocuboids [59]. In this case, the desire for active catalytic crystalline surfaces evolved into the generation of differently shaped nanoparticles. If one were to carve out similarly shaped Au nanoparticles from the top down, *e.g.*, using electron beam lithography, it is unlikely that these particles would have the same catalytic properties as the ones where the bottom up growth was manipulated to reveal the higher index facets. The relative surface areas of the higher energy facets determine the catalytic properties, not the overall shape of the nanoparticle. On the other hand, if one is only interested in the optical properties of the Au nanoparticles, then the bottom up and top down methods could be substituted for one other, as shape is more important than the crystallinity of the exposed facets in determining the energetics of the localized surface plasmon resonances.

2.1.4 Anisotropic Nanoparticle Structures

At the nanoscale, the shape, crystallinity, and emergent properties of a nanoparticle are all interrelated, and as demonstrated in the following sections, nanoparticles come in all shapes and sizes, where each particle can possess properties unique to

their geometry [4–7, 27, 29, 30, 47]. These sections are not exhaustive, with scientists stretching their imaginations and becoming more sophisticated every day in their design and application of particles in the nanoscale regime.

2.1.4.1 Spheres

Nanospheres are the most widespread shape that is used in nanomaterial manufacturing due to the increased thermodynamic stability of spheres compared to other shapes. They are isotropic, zero-dimensional materials whose properties are highly dependent on nanoparticle diameter. An increase in size leads to more red-shifted optical properties due to the decrease in electron confinement. Metal nanoparticles do not have a bandgap so electrons are delocalized and confined in the potential well of the nanoparticle, whereas semiconductor nanoparticles, or quantum dots, have a band gap in the valence band and conduction band that is dependent on size. As the quantum dots increase in size, more atomic orbitals contribute to the conduction and valence bands, leading to a decrease in band gap size and a red shift in fluorescence emission. A variety of hollow nanospheres have also been created [60–63]. Hollow nanoparticles can be used as carriers to protect or selectively deliver a high load of toxic material in therapeutic applications. In one example, hollow mesoporous silica nanoparticles were loaded with a radionucleotide and a photosensitizer to encapsulate and deliver them to tumors [61]. Once inside of the cell, the photosensitizer reacted with the nucleotide to create reactive oxygen species to kill the cell as well as emit light as a photodynamic therapy light source [61].

Anisotropy can be achieved in isotropic nanoparticle shapes, such as spheres, through the creation of multicomponent nanoparticles. The size, shape, and composition dependent properties of nanoparticles can be combined to create nanoparticles with different chemical or physical domains [64]. These can be used to accomplish new or more complex tasks. As shown in Fig. 2.10, nanoparticles with anisotropic compositions include core/shell nanoparticles, [19, 65–67] Janus nanoparticles, [63, 68, 69] and nanoparticles with island morphologies [70].

These structures generally preserve the properties of the individual components, leading to greater tunability and functionality [4–7, 25, 28, 30, 71]. In multifunctional nanoparticles, materials with unique optical signatures can be coupled to materials with desirable physical properties in a single nanostructure. For example, magnetic-plasmonic core/shell nanoparticles have magnetic functionality along with a plasmon band characteristic of the metal [72, 73]. The addition of metallic shells leads to a plasmon band that is dependent on the strength of the coupling of the plasmon band to the core material, which is dependent on the shell thickness [73]. The development of nanomaterials with multimodal functionalities opens up new avenues for creating structures with anisotropic functionalities for applications such as nanomotors, [63, 74, 75], surface plasmon resonance sensors [76] and optical imaging.

2.1.4.2 Rods, Wires and Tubes

Nanorods, nanowires and nanotubes have an increased length in one direction that leads to electron delocalization in the lateral dimension. Elongated nanostructures have properties that are dependent on aspect ratio (r = length/width). One-dimensional nanoparticles have been synthesized from a large range of materials including: metals, (Ag, Au, Pd, Pt, Rh, Cu, etc.), semiconductors (CdSe, CdTe, etc.), carbon-based materials etc. and have been applied to surface enhanced Raman Spectroscopy (SERS), light emitting diodes, energy transfer applications, [24] drug delivery applications, catalysis, [77] among others. Nanowires (NW) and nanotubes (NT) have been used as field effect transistors to record, stimulate and inhibit neuronal signals, [78] biological and chemical sensors, [22] nanoantennas, [79] waveguides, photovoltaics, [80] lasers, [81] and electronics [34, 82]. Nanowires have potential for nanoelectronics or "lab-on-a-chip" applications due to their small sizes that allow for non-invasive probes in biological applications, the ability to transduce signals across an electrode and ability to be passivated to prevent corrosion of metal junctions that typically lead to electronic failure [78]. Nanorods have an elongated *c*-axis that causes the movement of charge carriers to be asymmetric, leading to more mobility in one dimension. In semiconductor nanorods, or quantum rods (QRs), this typically leads to a lower quantum yield due to the longer electron-hole separation that increases the recombination time and decreases recombination rate. Once the electron-hole pair is separated, there is a chance that the charge carriers can react at the interface instead of with the other charge carrier, which is beneficial for applications that require charge separation such as catalysis and solar cells. QRs and gold nanorods (AuNRs) also absorb and emit linearly polarized light [21]. The internal polarization of nanorods is not completely orthogonal to the surface normal along its entire length, leading to different surface charges that can significantly affect the properties of the nanorod [83]. In metal nanorods, a longitudinal surface plasmon peak arises that can be tuned over the visible to the near-IR region, depending on aspect ratio [26]. The elongated shape gives nanorods a higher surface area, which has a positive impact on surface based applications. For example, CeO_2-Cu_xO_y nanocubes and nanorods were evaluated for the photochemical production of H_2 from hydrazine [77]. The rods were found to have the highest photocatalytic activity due to the higher surface area of rods compared to cubes [77].

Carbon nanotubes have been gaining increasing attention due to their unique structures and high mechanical strength, which is important for electronic applications. Single walled carbon nanotubes (SWCNTs) are made up of graphene like structures in the form of a tube, whereas multi-walled carbon nanotubes (MWCNTs) are made up on one or more concentric SWCNTs, which increase the mechanical stability of the nanotubes (NTs). Carbon nanotubes can act as a metal or a semiconductor, depending on the chirality, or the orientation of the carbon's crystal lattice compared to the tube's central axis. Metal SWCNTs do not display

fluorescence and they quench the fluorescence from neighboring semiconductor SWCNTs [84]. Gold nanowires have also been found to be up to 100 times mechanically stronger than bulk, with strength increasing for decreasing diameter [85].

Nanowires are typically grown orthogonally onto substrates, so nanowire arrays can be created to take advantage of their synergistic effects. For example, in semiconductor nanowires, increasing the nanowire diameter led to an increase in photocurrent density due to the increased light absorption [80]. The small diameter of these nanowires, which is much smaller than carrier diffusion lengths, can give nanowires the ability to approach the Shockley-Queisser efficiency limit for solar cells [80]. The small diameter of nanowires coupled with the longer length that allows for high mechanical stability compared to bulk, increased photocurrent and ability to be passivated with a variety of materials and molecules gives nanowires significant potential for their incorporation in electronics, sensors, waveguides, among others.

2.1.4.3 Cubes, Hexagons, Triangles

Nanocubes (NCs), nanohexagons (NHx) and nanotriangles have multiple corners that lead to accumulation of dipoles. NCs with sharp and rounded corners have been synthesized and they display multiple SPR peaks, as shown in Fig. 2.11 [18, 86, 87].

The appearance of sharp edges has been found to cause charge accumulation at the corners and lead to stronger dipoles inside of the nanoparticle that lead to interesting features in light scattering and absorption [18]. Due to their cubic shape, nanocubes (NCs) can maximize packing and assemble into lattice matched

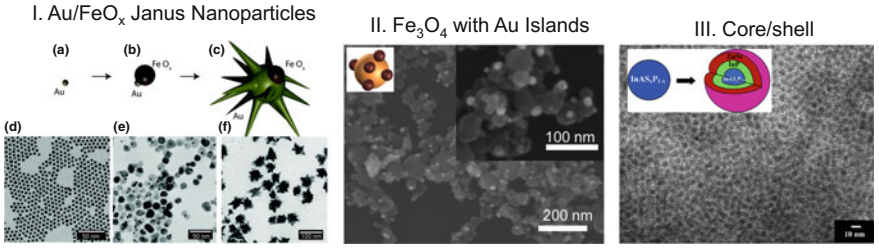

Fig. 2.10 **I**. Au/FeO_x Janus nanoparticles (**a**) Au core, (**b**) Au-FeO_x Janus precursor, (**c**) final Au/FeO_x Janus particles, Open access from Ref. [69]. Published by the Royal Society of Chemistry (RSC); **II**. Fe_3O_4 nanoparticles with Au "island" domains, reproduced with permission from Ref. [70]. Copyright © 2016 American Chemical Society. **III.** Schematic and TEM of core/shell InAsP/InP/ZnSe nanoparticles, reproduced with permission from J. Am. Chem. Soc., 2005. 127(30): pp. 10526–10532. Copyright © 2015 American Chemical Society

superstructures for electronic and magnetic applications [88]. The different facets of nanocubes also have different activities for applications such as catalysis. Compared to other morphologies, nanocube cobalt oxides have been found to have the highest activity for the oxidation of 1,2-dichloroethane, one of the most common pollutants in waste streams [89]. Planar nanoparticles such as metallic NCs coupled to dielectric substrates display stronger substrate induced hybridization compared to spherical nanoparticles due to the larger surface area that is coupled to the dielectric material [76]. This led to the appearance of a new narrow and highly sensitive plasmon mode with powerful consequences for very sensitive surface plasmon based sensing [76]. The increased number of hot spots on the corners compared to rods and spheres generally leads to an increase in reactivity in the cubes, triangles and hexagons.

2.1.4.4 Branched and Other Shapes

Polyhedral and planar branched nanoparticles, such as stars and tetrapods [19, 33, 49, 52, 90, 91], have been created to enhance catalysis, gas sensing, and surface enhanced Raman Spectroscopy (SERS) [4, 7, 28, 29, 45, 90]. The unique structure of branched nanoparticles leads to properties that depend on the composition, length, width and number of arms. Tips, edges and vertices can act as hot spots for electric field enhancement, leading to increased sensing properties and reactivities. Branched nanoparticles tend to have absorption or emission in the red and near-IR region. The plasmon bands for star-like metal nanoparticles are the result of the hybridization of the plasmons from the core and the tips [40, 92].

Particles with a larger number of branches, such as spiky gold nanoshells, have been used in SERS sensing due to the larger number of hot spots at the junctions of the arms and at the tips of the spikes [40, 93]. As shown in Fig. 2.12, the spiky gold nanoshells showed a SERS response at lower concentrations than the smooth gold shells. These spiky structures also showed a significantly higher scattering and a surface plasmon resonance (SPR) band that was dependent on the length of the spikes, where longer spikes led to a red-shift in the band [40]. Modeling of the electric field in the spiky shells showed that the electric field is localized at the tip of the cones and the locations where spikes overlap [40]. The SPR band is believed to be a resonance that localizes mostly at the junctions of the arms [40].

CdSe/CdS nanotetrapods were found to have a higher absorption cross section, indicating that the tetrapod arms absorb more light and act as a more efficient light harvesting system compared to QRs [49]. The width of the tetrapod arms had more of an effect on quantum yield (QY) than length of the arms. For the CdSe/CdS system, the electron-hole pair is confined to the core, but quantum confinement

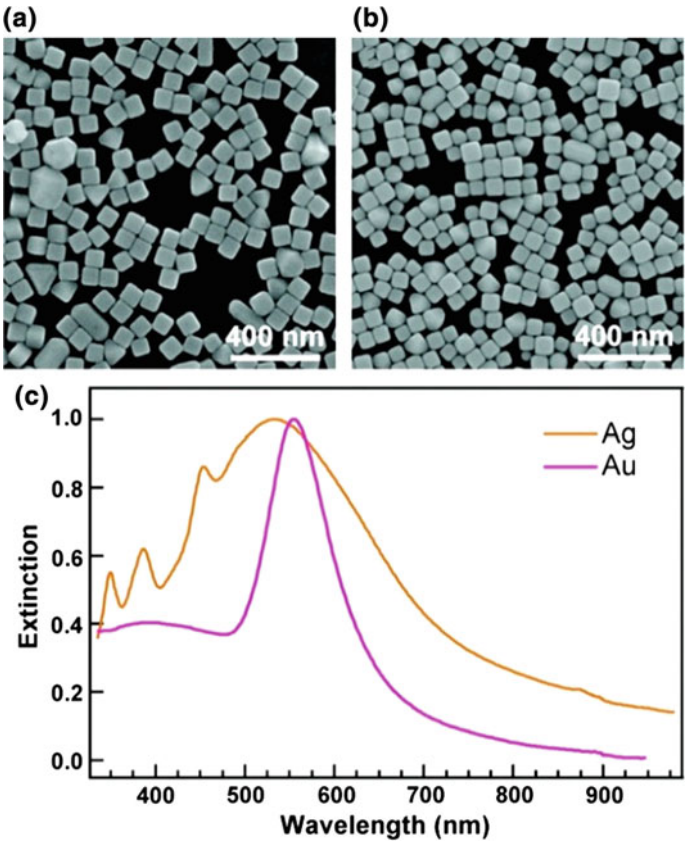

Fig. 2.11 (**a**, **b**) SEM images of the Ag and Au nanocubes, respectively. (**c**) Extinction spectra of the Ag and Au nanocubes. Reproduced with permission from Ref. [87]. Copyright © 2011 American Chemical Society

causes stronger electron localization at the branch in the narrower arms compared to the thicker arms, leading to higher QY and absorption in tetrapods with narrower arms [49]. The unique morphologies of branched nanoparticles that allow for more "hot spots" and light interactions has led to the development of a wide variety of materials and shapes that have been investigated for sensing, SERS applications, and light harvesting systems.

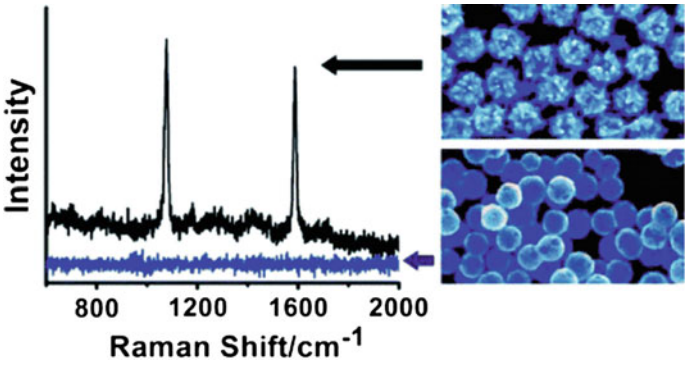

Fig. 2.12 SERS of spiky gold nanoshells (*black spectra*) compared to smooth gold nanoshells (*blue spectra*). Reproduced with permission from Ref. [40]. Copyright © 2012 American Chemical Society

2.2 Conclusions

A plethora of nanoparticle shapes have been created and employed for biological delivery and sensing, catalysis, and electronics. The chemical and physical properties are highly dependent on composition and morphology; various experimental and theoretical works have gone into exploring the nature of these properties to exploit them to their full potential.

References

1. https://www.epa.gov/chemical-research/research-nanomaterials.
2. Masciangioli, T., and W.-X. Zhang. 2003. Peer Reviewed: Environmental Technologies at the Nanoscale. *Environmental Science and Technology* 37 (5): 102A–108A.
3. Mazzola, L. 2003. Commercializing Nanotechnology. *Nature Biotechnology* 21 (10): 1137.
4. Hunyadi, S.E. 2007. Nanoengineered Materials: Synthesis, Design, Functionalization and Chemical Sensing Applications. In *Department of Chemistry and Biochemistry*, p. 262. Columbia, SC: University of South Carolina.
5. Hunyadi Murph, S.E., et al. 2012. Metallic and Hybrid Nanostructures: Fundamentals and Applications. In *Applications of Nanomaterials*, ed. J.N. Govil. USA: Studium Press LLC.
6. Murphy, C.J., et al. 2005. Anisotropic Metal Nanoparticles: Synthesis, Assembly, and Optical Applications (Feature Article; a Top Five ACS article by citations, National Chemistry Week, 2007). *Journal of Physical Chemistry B* 109: 13857–13870.
7. Murphy, C.J., et al. 2006. One-Dimensional Colloidal Gold and Silver Nanostructures. *Inorganic Chemistry* 45 (19): 7544–7554.
8. Fedlheim, D.L, and C.A. Foss. 2001. In: *Metal Nanoparticles: Synthesis, Characterization, and Applications*, Edited By D.L. Fedlheim and C.A. Foss. New York: Marcel Dekker Inc.
9. Murphy, C.J., et al. 2008. Chemical Sensing and Imaging with Metallic Nanorods. *Chemical Communications* 4 (554–557): 554.

10. Kuchibhatla, S.V.N.T., et al. 2007. One Dimensional Nanostructured Materials. *Progress in Materials Science* 52 (5): 699–913.
11. Tiwari, J.N., R.N. Tiwari, and K.S. Kim. 2012. Zero-dimensional, one-dimensional, two-dimensional and three-dimensional nanostructured materials for advanced electrochemical energy devices. *Progress in Materials Science* 57 (4): 724–803.
12. Hunyadi Murph, S.E., et al. 2011. Synthesis, Functionalization, Characterization and Application of Controlled Shape Nanoparticles in Energy Production. In *Fluorine-Related Nanoscience with Energy Applications*, ed. D.J. Nelson, and C.N. Brammer.
13. Hunyadi Murph, S.E., et al. 2011. Tuning of Size and Shape of Au-Pt Nanocatalyst for Direct Methanol Fuel Cells. *Journal of Nanoparticle Research* 13 (6347–6364): 6347.
14. Roduner, E. 2006. Size Matters: Why Nanomaterials are Different. *Chemical Society Reviews* 35 (7): 583–592.
15. Valden, M., X. Lai, and D.W. Goodman. 1998. Onset of Catalytic Activity of Gold Clusters on Titania with the Appearance of Nonmetallic Properties. *Science* 281 (5383): 1647–1650.
16. Chen, M., and D. Goodman. 2004. The Structure of Catalytically Active Gold on Titania. *Science* 306 (5694): 252–255.
17. Kim, S.-W., et al. 2002. Fabrication of Hollow Palladium Spheres and their Successful Application to the Recyclable Heterogeneous Catalyst for Suzuki Coupling Reactions. *Journal of the American Chemical Society* 124 (26): 7642–7643.
18. Wiley, B., S.H. Im, Z. Li, J. McLellan, A. Siekkinen, and Y. XIa. 2006. Maneuvering the Surface Plasmon Resonance of Silver Nanostructures through Shape-Controlled Synthesis. *The Journal of Physical Chemistry B* 110: 15666–15675.
19. Meng, M., et al. 2016. Integration of Kinetic Control and Lattice Mismatch to Synthesize Pd@AuCu Core-Shell Planar Tetrapods with Size-Dependent Optical Properties. *Nano Letters* 16: 3036–3041.
20. Wiley, B., et al. 2005. Shape-Controlled Synthesis of Metal Nanostructures: The Case of Silver. *Chemistry A European Journal* 11: 454–463.
21. Hadar, I., G.B. Hitin, A. Sitt, A. Faust, and U. Banin. 2013. Polarization Porperties of Semiconductor Nanorod Heterostructures: From Single Particles to Ensemble. *The Journal of Physical Chemistry Letters* 4: 502–507.
22. Cui, Y., et al. 2001. Nanowire Nanosensors for Highly Sensitive and Selective Detection of Biological and Chemical Species. *Science* 293 (5533): 1289–1292.
23. Giblin, J., and M. Kuno. 2010. Nanostructure Absorption: A Comparative Study of Nanowire and Colloidal Quantum Dot Absorption Cross Sections. *The Journal of Physical Chemistry Letters* 1: 3340–3348.
24. Halivni, S., A. Sitt, I. Hadar, and U. Banin. 2012. Effect of Nanoparticle Dimensionality on Fluorescence Resonance Energy Transfer in Nanoparticle-Dye Conjugated Systems. *ACS Nano* 6 (3): 2758–2765.
25. Hunyadi Murph, S.E., and C.J. Murphy. 2006. Tunable One-Dimensional Silver-Silica Nanopeapod Architectures. *The Journal of Physical Chemistry B* 110: 7226–7231.
26. Zhang, Q., L. Han, H. Jing, D.A. Blom, Y. Lin, H.L. Zin, and H. Wang. 2016. Facet Control of Gold Nanorods. *ACS Nano* 10 (2): 2960–2974.
27. Unrine, J., P. Bertsch, and S.E. Hunyadi. 2008. Bioavailability, Trophic Transfer and Toxicity of Manufactured Metal and Metal Oxide Nanoparticles in Terrestrial Environments. In *Nanoscience and Nanotechnology: Environmental and Health Impacts*, ed. V. Grassian, 343–364. New Jersey: Wiley.
28. Hunyadi, S.E., and C.J. Murphy. 2006. Bimetallic Silver-Gold Nanowires: Fabrication and Use in Surface- Enhanced Raman Scattering. *Journal of Materials Chemistry* 16 (Special Issue: Anisotropic Nanoparticles): 3929–3935.
29. Hunyadi Murph, S.E., and C.J. Murphy. 2013. Patchy Silica-Coated Silver Nanowires as SERS Substrates. *Journal of Nanoparticle Research* 15 (6): 1607.
30. Hunyadi Murph, S.E., et al. 2012. Manganese- Doped Gold Nanoparticles as Positive Contrast Agents for Magnetic Resonance Imaging (MRI). *Journal of Nanoparticle Research* 14: 658–659.

31. Chen, H., et al. 2008. Shape- and Size- Dependent Refractive Index Sensitivity of Gold Nanoparticles. *Langmuir* 24: 5233–5237.
32. Chen, H., et al. 2009. Shape-Dependent Refractive Index Sensitivities of Gold Nanocrystals with the Same Plasmon Resonance Wavelength. *The Journal of Physical Chemistry C* 113: 17691–17697.
33. Tulun, F.R., S. Öztürk, and Z.Z. Öztürk. 2016. The NO_2 Sensing Properties of the Sensors Done with Nano-Tetrapods. *Acta Physica Polonica A* 129: 797–799.
34. Gudiksen, M.S., et al. 2002. Growth of Nanowire Superlattice Structures for Nanoscale Photonics and Electronics. *Nature* 415: 617–620.
35. Langhammer, C., I. Zorić, B. Kasemo, and B.M. Clemens. 2007. Hydrogen Storage in Pd Nanodisks Characterized with a Novel Nanoplasmonic Sensing Scheme. *Nano Letters* 7: 3122–3127.
36. Subhramannia, M., and V.K. Pillai. 2008. Shape-Dependent Electrocatalytic Activity of Platinum Nanostructures. *Journal of Materials Chemistry* 18: 5858–5870.
37. Chithrani, B.D., A.A. Ghazani, and W.C.W. Chan. 2006. Determining the Size and Shape Dependence of Gold Nanoparticle Uptake into Mammalian Cells. *Nano Letters* 6: 662–668.
38. Huang, X., et al. 2010. The Effect of the Shape of Mesoporous Silica Nanoparticles on Cellular Uptate and Cell Function. *Biomaterials* 31 (3): 438–448.
39. Khon, E., K. Lambright, R. Khnayzer, P. Moroz, D. Perera, E. Butaeva, S. Lambright, F. Castellano, and M. Zamkov. 2013. Improving the Catalytic Activity of Semiconductor Nanocrystals through Selective Domain Etching. *Nano Letters* 13: 2016–2023.
40. Sanchez-Gaytan, B.L., et al. 2012. Spiky Gold Nanoshells: Synthesis and Enhanced Scattering Properties. *The Journal of Physical Chemistry C* 116: 10318–10324.
41. Sitt, A., A. Salant, G. Menagen, and U. Banin. 2011. Highly Emissive Nano Rod-in-Rod Heterostructures with Strong Linear Polarization. *Nano Letters* 11: 2054–2060.
42. Ming, T., et al. 2009. Strong Polarization Dependence of Plasmon-Enhanced Fluorescence on Single Gold Nanorods. *Nano Letters* 9: 3896–3903.
43. Hu, J., et al. 2001. Linearly Polarized Emission from Colloidal Semiconductor Quantum Rods. *Science* 292: 2060–2063.
44. Near, R.D., S.C. Hayden, R.E. Hunter, D. Thackston, and M. El-Sayed. 2013. Rapid and Efficient Prediction of Optical Extinction Coefficients for Gold Nanospheres and Gold Nanorods. *The Journal of Physical Chemistry C* 117: 23950–23955.
45. Song, C., et al. 2012. Gold-Modified Silver Nanorod Arrays: Growth Dynamics and Improved SERS Properties. *Journal of Materials Chemistry* 22: 1150–1159.
46. Hunyadi Murph, S.E., et al. 2015. A Possible Oriented Attachment Growth Mechanism for Silver Nanowire Formation. *Crystal Growth & Design* 15: 1968–1974.
47. Tao, C.G., et al. 2007. Surface Morphology and Step Fluctuations on Silver Nanowires. *Surface Science* 601: 4939–4943.
48. Lucas, M., et al. 2008. Plastic Deformation of Pentagonal Silver Nanowires: Comparison Between AFM Nanoindentation and Atomistic Simulations. *Physical Review B* 77: 2452014–2454201.
49. Talapin, D.V., et al. 2007. Seeded Growth of Highly Luminscent CdSe/CdS Nanoheterostructures with Rod and Tetrapod Morphologies. *Nano Letters* 7: 2951–2959.
50. Scarabelli, L., et al. 2015. A "Tips and Tricks" Practical Guide to the Synthesis of Gold Nanorods. *The Journal of Physical Chemistry Letters* 6: 4270–4279.
51. Sun, Y., and Y. Xia. 2002. Shape-Controlled Synthesis of Gold and Silver Nanoparticles. *Science* 298: 2176–2179.
52. Manna, L., et al. 2003. Controlled Growth of Tetrapod-Branced Inorganic Nanocrystals. *Nature Materials* 2: 382–385.
53. Lu, X., T.T. Tran, and W. Zhang. 2013. Shape-Selective Effect of Foreign Metal Ions on Growth of Noble Metal Nanocrystals with High-Index Facets. *Journal of Chemical Engineering and Process Technology* 1: 1009–1016.

54. Lyu, L., and M.H. Huang. 2011. Investigation of Relative Stability of Different Facets of Ag_2O Nanocrystals Through Face-Selective Etching. *The Journal of Physical Chemistry C* 115 (36): 17768–17773.
55. Tachikawa, T., S. Yamashita, and T. Majima. 2011. Evidence for Crystal-Face-Dependent TiO_2 Photocatalysis from Single-Molecule Imaging and Kinetic Analysis. *Journal of the American Chemical Society* 133: 7197–7204.
56. Schmidt, E., et al. 2009. Platinum Nanoparticles: The Crucial Role of Crystal Face and Colloid Stabilizer in the Diastereoselective Hydrogenation of Cinchonidine. *Chemistry European Journal* 16 (7): 2181–2192.
57. Ikeda, K., S. Suzuki, and K. Uosaki. 2011. Crystal Face Dependent Chemical Effects in Surface-Enhanced Raman Scattering at Atomically Defined Gold Facets. *Nano Letters* 11: 1716–1722.
58. Han, X., et al. 2009. Synthesis of Tin Dioxide Octahedral Nanoparticles with Exposed High-Energy 221 Facets and Enhanced Gas-Sensing Properties. *Angewandte Chemie International Edition* 121 (48): 9344–9347.
59. Zhang, Q., et al. 2015. Faceted Gold Nanorods: Nanocuboids, Convex Nanocuboids, and Concave Nanocuboids. *Nano Letters* 15 (6): 4161–4169.
60. Lal, S., et al. 2002. Light Interaction between Gold Nanoshells Plasmon Resonance and Planar Optical Waveguides. *The Journal of Physical Chemistry B* 106: 5609–5612.
61. Kamkaew, A., et al. 2016. Cerenkov Radiation Induced Photodynamic Therapy Using Chlorin e6-Loaded Hollow Mesoporous Silica Nanoparticles. *ACS Applied Materials & Interfaces* 8 (40): 26630–26637.
62. Son, S.J., X. Bai, and S.B. Lee. 2007. Inorganic Hollow Nanoparticles and Nanotubes in Nanomedicine: Part 2: Imaging, Diagnostic, and Therapeutic Applications. *Drug Discovery Today* 12: 657–663.
63. Ma, X., et al. 2015. Enzyme-Powered Hollow Mesoporous Janus Nanomotors. *Nano Letters* 15: 7043–7050.
64. Carbone, L., and P.D. Cozzoli. 2010. Colloidal Heterostructured Nanocrystals: Synthesis and Growth Mechanisms. *Nano Today* 5: 449–493.
65. Lyon, J.L., D.A. Fleming, M.B. Stone, P. Schiffer, and M.E. Williams. 2004. Synthesis of Fe oxide Core/Au Shell Nanoparticles by Iterative Hydroxylamine Seeding. *Nano Letters* 4 (4): 719–723.
66. Ji, T., et al. 2001. Preparation, Characterization, and Application of Au-shell/Polystyrene Beads and Au-shell/Magnetic Beads. *Advanced Materials* 13 (16): 1253–1256.
67. Harpeness, R., and A. Gedanken. 2004. Microwave Synthesis of Core-Shell Gold/Palladium Bimetallic Nanoparticles. *Langmuir* 20: 3431–3434.
68. Kostevsek, N., et al. 2016. The One-Step Synthesis and Surface Functionalization of Dumbbell-Like Gold-Iron Oxide Nanoparticles: A Chitosan-Based Nanotheranostic System. *Chemical Communications* 52: 378–381.
69. Reguera, J., et al. 2016. Synthesis of Janus Plasmonic-Magnetic, Star-Sphere Nanoparticles, and Their Application in SERS Detection. *Faraday Discussions* 191: 47–59.
70. Larsen, G.K., W. Farr, and S.E.H. Murph. 2016. Multifunctional Fe_2O_3-Au Nanoparticles with Different Shapes: Enhanced Catalysis, Photothermal Effects, and Magnetic Recyclability. *The Journal of Physical Chemistry C* 120 (28): 15162–15172.
71. Hunyadi, S.E., and C.J. Murphy. 2009. Synthesis and Characterization of Silver-Platinum Bimetallic Nanowires and Platinum Nanotubes. *Journal of Cluster Science* 20: 319–330.
72. Kwizera, E.A., et al. 2016. Size- and Shape-Controlled Synthesis and Properties of Magnetic-Plasmonic Core-Shell Nanoparticles. *The Journal of Physical Chemistry C* 120: 10530–10546.
73. Levin, C.S., et al. 2009. Magnetic-Plasmonic Core-Shell Nanoparticles. *ACS Nano* 3 (6): 1379–1388.
74. Liu, R., and A. Sen. 2011. Autonomous Nanomotor Based on Copper-Platinum Segmented Nanobattery. *Journal of the American Chemical Society* 133: 20064–20067.

75. Kagan, D., P. Calvo-Marzal, S. Balasubramanian, S. Sattayasamitsathit, K.M. Manesh, G. Flechsig, and J. Wang. 2009. Chemical Sensing Based on Catalytic Nanomotors: Motion-Based Detection of Trace Silver. *Journal of the American Chemical Society* 131: 12082–12083.
76. Zhang, S., et al. 2011. Substrate-Induced Fano Resonances of a Plasmonic Nanocube: A Route to Increased Sensitivity Localized Surface Plasmon Resonance Sensors Revealed. *Nano Letters* 11: 1657–1663.
77. Clavijo-Chaparro, S.L., et al. 2016. Water Splitting Behavior of Copper-Cerium Oxide Nanorods and Nanocubes Using Hydrazine as a Scavenging Agent. *Journal of Molecular Catalysis A: Chemical* 423: 143–150.
78. Patolsky, F., et al. 2006. Detection, Stimulation and Inhibition of Neuronal Signals with High-Density Nanowire Transistor Arrays. *Science* 313: 1100–1104.
79. Day, J.K., et al. 2014. Standing Wave Plasmon Modes Interact in an Antenna-Coupled Nanowire. *Nano Letters* 15: 1324–1330.
80. LaPierre, R.R., et al. 2013. III-V Nanowire Photovoltaics: Review of Design for High Efficiency. *Rapid Research Letters* 7 (10): 815–830.
81. Huang, M.H., et al. 2001. Room-Temperature Ultraviolet Nanowire Nanolasers. *Science* 292 (5523): 1897–1899.
82. Kind, M., et al. 2002. Nanowire Ultraviolet Photodetectors and Optical Switches. *Advanced Materials* 14 (2): 158–160.
83. Krishnan, R., M. Hahn, Z. Yu, J. Silcox, P. Fauchet, and T. Krauss. 2004. Polarization Surface-Charge Density of Single Semiconductor Quantum Rods. *Physical Review Letters* 92 (21): 216803.
84. Kozák, O., M. Sudolská, G. Pramanik, P. Cígler, M. Otyepka, and R. Zbořil. 2016. Photoluminescent Carbon Nanostructures. *Chemistry of Materials* 28: 4085–4128.
85. Wu, B., A. Heidelberg, and J.J. Boland. 2005. Mechanical Properties of Ultrahigh-Strength Gold Nanowires. *Nature Materials* 4: 525–529.
86. McLellan, J.M., et al. 2007. The SERS ACTIVIty of a Supported Ag Nanocube Strongly Depends on its Orientation Relative to Laser Light. *Nano Letters* 7 (4): 1013–1017.
87. Lee, Y.H., et al. 2011. Refractive Index Sensitivities of Nobel Metal Nanocrystals: The Effects of Multipolar Plasmon Resonances and the Metal Type. *Journal of Physical Chemistry C* 115 (16): 7997–8004.
88. Li, W., et al. 2013. Metal Ions to Control the Morphology of Semiconductor Nanoparticles: Copper Selenide Nanocubes. *Journal of the American Chemical Society* 135: 4664–4667.
89. González-Prior, J., et al. 2016. Oxidation of 1,2-dichloroethane Over Nanocube-Shaped Co_3O_4 Catalysts. *Applied Catalysis, B: Environmental* 199: 384–393.
90. Watson, A.M., X. Zhang., R. Alcaraz de la Osa., J.M. Sanz., F. González., F. Moreno., G. Finkelstein., J. Liu., and H.O. Everitt. 2015. Rhodium Nanoparticles for Ultraviolet Plasmonics. *Nano Letters* 15: 1095–1100.
91. Biacchi, A.J., and R.E. Schaak. 2011. The Solvent Matters: Kinetic versus Thermodynamic Shape Control in the Polyol Synthesis of Rhodium Nanoparticles. *ACS Nano* 5: 8089–8099.
92. Hao, F., et al. 2007. Plasmon Resonances of a Gold Nanostar. *Nano Letters* 7 (3): 729–732.
93. Lascola, R.J., C.S. McWhorter., and S.H. Murph. 2015. *Surface enhanced Raman scattering spectroscopic waveguide*. USPTO, Savannah River Nuclear Solutions, Llc, Aiken.

http://www.springer.com/978-3-319-59661-7

Anisotropic and Shape-Selective Nanomaterials
Structure-Property Relationships
Hunyadi Murph, S.E.; Larsen, G.K.; Coopersmith, K.J.
(Eds.)
2017, X, 470 p. 228 illus., 160 illus. in color., Hardcover
ISBN: 978-3-319-59661-7